coatings

MDPI

Article

Study on Fatigue Performance of 2200 MPa High-Strength Wire of Main Cables Based on FE-SAFE

Hongtao Li [1], Zhubing Zhou [2], Sen Liu [3], Leyong Wei [4], Jun Zhao [2] and Han Su [3,*]

[1] Jiangsu Provincial Transportation Engineering Construction Bureau, Nanjing 210004, China
[2] Jiangsu Fasten Cable Co., Ltd., Jiangyin 214433, China
[3] School of Civil Engineering, Beijing Jiaotong University, Beijing 100044, China
[4] CCCC Highway Consultants Co., Ltd., Beijing 100088, China
* Correspondence: hansu@bjtu.edu.cn

Abstract: In order to estimate the fatigue life of 2200 MPa high-strength steel wire for main cables at the outlet of the cable saddle, a fatigue loading test of a single steel wire was designed, and the value of the friction coefficient in finite element simulation and the scale factor in fatigue life analysis were determined. The fatigue life of the steel wire was analyzed by two-stage modelling. The results showed that the fatigue life of steel wire can be simulated effectively when the friction coefficient is 0.21 and the scale factor is 1.15. The fatigue life of 2200 MPa main cable wire at the saddle outlet is 4.78 million loading cycles. The research results laid a foundation for practical engineering application of high-strength steel wire for 2200 MPa main cables.

Keywords: suspension bridge; main cable; high-strength wire; fatigue performance; cable saddle

Citation: Li, H.; Zhou, Z.; Liu, S.; Wei, L.; Zhao, J.; Su, H. Study on Fatigue Performance of 2200 MPa High-Strength Wire of Main Cables Based on FE-SAFE. *Coatings* **2023**, *13*, 646. https://doi.org/10.3390/coatings13030646

Academic Editor: Giorgos Skordaris

Received: 14 February 2023
Revised: 7 March 2023
Accepted: 13 March 2023
Published: 19 March 2023

1. Introduction

The main cable is an important load-bearing component of suspension bridge, and its mechanical properties are an important basis for bridge design, operation, and maintenance. The core component of the main cable is high-strength galvanized steel wire, which is mainly produced by cold-drawn pearlite wire rods [1–3]. With the increasing span of bridges, the research and development of higher-strength steel wire has been the focus of attention in the industry. In China, 20 years ago, the high-strength steel wire used for the main cables of suspension bridges was no more than 1670 MPa. With the improvement of various technical means such as alloying, the sorbite content of pearlite wire rods produced by large-scale industry has increased, and the spacing of the sorbite layer is more uniform, which also makes the strength of high-strength steel wire produced by industry improve. From the 1770 MPa adopted by the Xihoumen Bridge [4] to the 1960 MPa adopted by the Second Humen Bridge [5], the research and application of high-strength steel wire have made great progress. With the increase of the strength of the main cable wire, more and more attention has been paid to the fatigue property of the wire, especially the main cable wire located at the exit of the saddle. It has been shown that the lower steel wire at the exit of the cable saddle is most prone to fatigue failure due to fatigue load and fretting wear. Fretting wear is mainly affected by contact conditions of friction surfaces (including normal stress, shear stress and friction coefficient) [6].

At present, some scholars have studied the mechanical properties of high strength main cable strands. Lu [7] verified the bearing capacity of 1960 MPa galvanized alloy coated steel wire main cable strand through static load test. Chen [8] introduced the 2060 MPa multi-alloy plated wire strand for the Lingdingyang Bridge. For the main cable wire steel at the outlet position of the cable saddle, current studies mostly focus on the relative slip between the main cable and the cable saddle. Wang [9] and Su [10] confirmed that the friction coefficient between the main cable and the cable saddle should be 0.2 through experiments. Li [11] determined that the friction coefficient between the wire strands of

parallel preparation should be 0.215. Dai [12] analyzed the slip characteristics between the main cable strand and the cable saddle through tests and finite element simulation. In finite element simulation, the friction coefficient between the steel wire was set at 0.2, which could effectively simulate the test results. For the fatigue of the main cable wire at the saddle position, Guo [13] conducted 2 million fatigue performance tests on the main cable strand at 2100 MPa, and found that the wire break rate was less than 2% and there were no abnormal anchors. Anatomical observation of the cable strand after the test showed that the extrusion and rubbing between the wires in the cable strand was the main cause of the fatigue fracture of the wire, which indicated that the fatigue damage of the wires in the cable strand was a multi-axial fatigue problem.

Many scholars have studied the multi-axial fatigue problem, and the research methods are mainly divided into three categories: the multiaxial equivalent stress-strain amendment algorithm, energy method, and critical plane method. The multiaxial equivalent stress-strain amendment algorithm is an early method to solve the multi-axial fatigue problem based on uniaxial fatigue test. The combination of stress or strain is used as the damage parameter of multi-axial fatigue. The energy method is a multi-axial fatigue algorithm based on cyclic plastic deformation and plastic strain energy as damage parameters. Lee [14] proposed that the sum of elastic strain energy, and plastic strain energy was taken as the damage parameter based on Garud [15]. The critical plane method is considered to be the most effective method to solve the problem of multi-axis fatigue [16–20]. Brown [21] took maximum shear strain and positive strain on the plane of maximum shear strain as the parameters of fatigue damage. Fatemi [22] believed that stress must be introduced into the damage parameters to describe the fatigue non-proportional hardening phenomenon and proposed to take the maximum shear strain and the normal stress on the plane of the maximum shear strain as the control parameters of fatigue damage. Zhao [23] established a multi-axial fatigue life model with elliptic equation, taking the maximum shear strain amplitude as the critical plane. Wu [24] took the sum of the maximum shear strain amplitude and its modified SWT parameter in the corresponding plane as the multi-axis fatigue damage control parameter. The research on multi-axis fatigue of high-strength steel wire mainly focuses on the fretting fatigue phenomenon caused by the contact of wire inside steel strand. Jia [25] established the finite element model of steel strand through the parametric modeling method and analyzed the fatigue characteristics based on the multi-axis fatigue critical plane method. Ma [26] analyzed the fatigue of 1860 grade steel strand and obtained the S-N curve of 1860 grade steel strand. At present, there are many methods for fatigue analysis of complex stress distribution, among which, importing stress-strain results obtained by finite element calculation into FE-SAFE for analysis has been proved to be feasible and reliable and has been widely used in life analysis of various fatigue details [27,28].

Based on the above situation, this paper firstly uses the S-N curve of the 1860 grade strand wire fitted by Marlin and determines the SN scale factor of FE-SAFE analysis of steel wire by the trial method. Then the fatigue test of a single steel wire is carried out to verify the rationality of the finite element simulation and fatigue life parameter selection (friction coefficient 0.215, SN scale factor 1.15). Finally, the fatigue life of the steel wire at the outlet position of the saddle was predicted by finite element modeling and FE-SAFE analysis.

2. Parameter Setting for Finite Element Simulation and Fatigue Life Analysis

2.1. General Situation of Fatigue Test of Single Steel Wire

The structure of a single steel wire fatigue test clamping device is shown in Figure 1a, which is mainly composed of test steel wire, a slotted clamping steel plate, and a bolt fastener. The slotted clamping steel plate is provided with a clamp groove for fixing the wire position, and the clamping length is 20 mm. One test steel wire and four filling steel wires are placed in the clamping steel plate slot. The device is equipped with two sets of M10 bolts and exerts pressure on the test steel wire through the bolt preloading force.

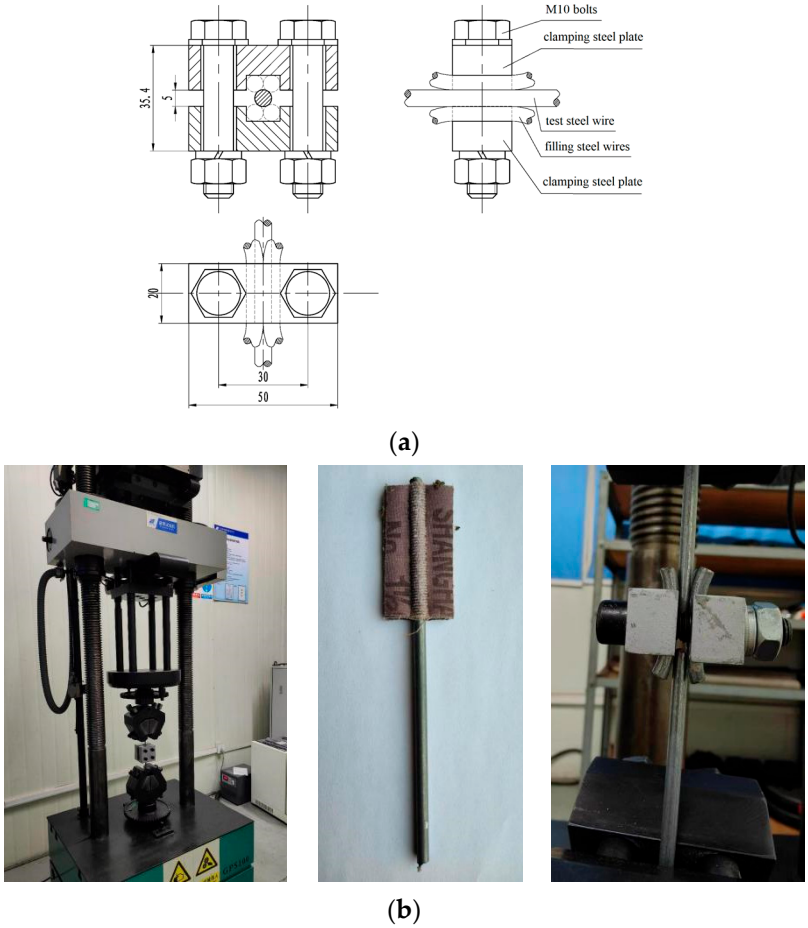

Figure 1. Single wire fatigue test. (**a**) Clamping device. (**b**) Test wire loading condition and failure mode.

The fatigue test of single steel wire was carried out on the GPS-100 high-frequency fatigue test machine. The two ends of the test steel wire were clamped and fixed respectively with the fixed end and the loading end of the machine. Before the fatigue test, the two ends of the wire were wrapped with sandpaper to increase the friction force and reduce the stress concentration of the wire caused by the clamp of the testing machine. The diameter of the test steel wire was 5.65 mm, and the bolt pre-tightening force of the two bolts was 2.6 kN. Figure 1b shows test wire loading condition and failure mode. The technical index of 2200 MPa is shown in Table 1, and the fatigue test data of steel wire are shown in Table 2. Under the clamping of steel plate, steel wire fractures at about 200,000 times fatigue loading, which is inconsistent with reality, indicating that the use of filling and holding the steel plate for clamping amplify the stress concentration of steel wire.

Table 1. Technical indicators of 2200 MPa steel wire.

Project	Unit	Magnitude
Tensile Strength	MPa	2209~2284
Non-proportional Extension Strength	MPa	1986~2120
Elasticity Modulus	MPa	$(2.00\sim2.10) \times 10^5$
Breaking Elongation Rate	%	5.0~6.0
Coating Quality	g/m^2	306~354
Relax Rate	%	2.6

Table 2. Fatigue loading test data of 2200-MPa-grade steel wire.

Number	Specification	σ_{max} /MPa	$\Delta\sigma$ /MPa	N	Fracture Location
1	5.65–2200	990	410	169,810	Clamping position
2	5.65–2200	990	410	276,988	Clamping position
3	5.65–2200	990	410	2,000,000	Unbroken stop
4	5.65–2200	990	410	152,247	Clamping position
5	5.65–2200	990	410	220,566	Clamping position
6	5.65–2200	990	360	186,767	Clamping position

2.2. Finite Element Simulation Based on ABAQUS

Figure 2a shows the geometric size of a single steel wire and a cylinder with a base radius of 2.825 mm and a height of 40 mm. The elastic modulus is 210,000 MPa, and eight-node linear hexahedron C3D8R solid element was employed. The boundary conditions were set as consolidation at one end (fixed end U1 = U2 = U3 = UR1 = UR2 = UR3 = 0) and no constraint at the other end (loading end). The axial force is applied to the loading end in the form of pressure; the first stage is −630.0 MPa, and the second stage is −990.0 MPa (negative values represent tensile stress and positive values represent compressive stress). In order to accurately simulate the test, the gripped steel plate and the filled steel wire under auxiliary loading are established. The size of the gripped steel plate is consistent with the actual size. The upper and lower surfaces of the two gripped steel plates are respectively subjected to pressure loads of 5.2 MPa to simulate the bolt preload, as shown in Figure 2b, which is the simulated fatigue loading test. (On the one hand, the area of the nut covers 2/3 of the clamping steel plate; on the other hand, the preload exerted by the bolt is small, and the preload is redistributed by the filling wire so the preload can be equivalent in this way.)

The contact property between test steel wire and filling steel wires is as follows: in tangential direction, penalty function method is adopted. According to Li's research on friction coefficient between parallel steel wires, friction coefficient is determined to be 0.215, and elastic sliding is not restricted. In the normal direction, hard contact is used. As the selection of contact surfaces in this model is based on geometry rather than elements, the contact type is selected as point-to-surface in surface-to-surface, the main surface is selected as the side of the loading center wire, and the secondary surface is selected as the side of the filling wire. In order to simplify the model, save calculation time, and improve convergence, it is considered that there is no relative displacement between the packed wire and the fixture; therefore, the packed wire and the fixture are bound. Figure 2c shows the grid division. The cell type of steel wire and reinforced steel plate is C3D8R. During the grid division, each steel wire is divided to obtain a structured grid.

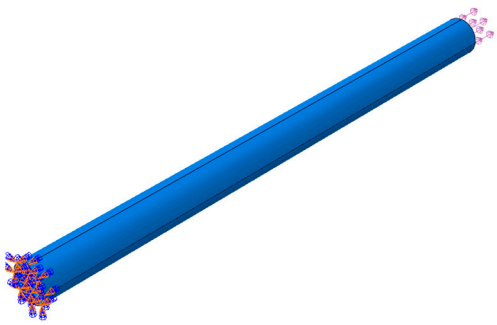

(**a**)

Figure 2. *Cont.*

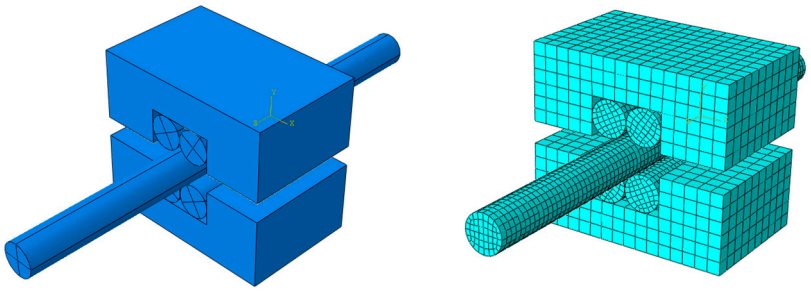

(**b**) (**c**)

Figure 2. (**a**) Simulation of fatigue loading test. (**b**) Axial load of single steel wire. (**c**) Schematic diagram of axial loading of single wire mesh generation.

2.3. Fatigue Life Analysis Based on FE-SAFE

Fatigue life analysis was carried out by FE-SAFE. The reasons for using this software for fatigue life analysis are: (1) easy operation process; (2) the built-in material library covers many fatigue life estimation methods; (3) existing materials can be modified and used; and (4) when using ABAQUS for finite element simulation, post-processing is convenient.

Considering the contact problem between steel wires, according to the S-N curve of steel strand obtained by Ma [26] through the test, the finite element model of a single steel wire under only axial load is established, and the SN-scale factor is determined by the test algorithm. The expression of S-N curve used in fatigue life prediction is:

$$\log N = 13.84 + 3.5 \log \Delta\sigma \quad (1)$$

Surface friction, residual stress, and SN-Scale factor are three important indexes of FE-SAFE for fatigue life analysis. The surface friction and residual stress are kept as default settings, and only SN scale factor is determined. According to the S-N curve of 1860 MPa steel strand studied by Ma [26], it can be determined that the upper limit of load corresponding to the specimen is 1145 MPa, and the fatigue life of steel strand with a stress range of 195.0 MPa is 663,000 loading cycles, namely $10^{5.829}$ times.

As shown in Figure 3a,b, the axial tensile stress of steel wire is 950 MPa in the first stage and 1145 MPa in the second stage. Figure 4 shows the fatigue life of steel wire simulated by FE-safe under axial fatigue load with the upper fatigue limit of 1145 MPa and the stress range of 195 MPa (SN scale factor is 1.15), the fatigue life of steel wire is $10^{5.829}$ times at all points, which is consistent with the test results of Ma [20], indicating that the fatigue life of the steel wire can be accurately simulated when the SN scale factor is 1.15.

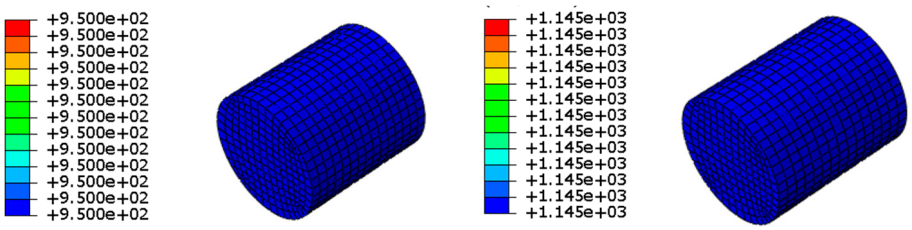

(**a**) (**b**)

Figure 3. Axial stress of the element in the span of steel wire (MPa). (**a**) The first stage (the lower limit of fatigue). (**b**) The second stage (fatigue limit).

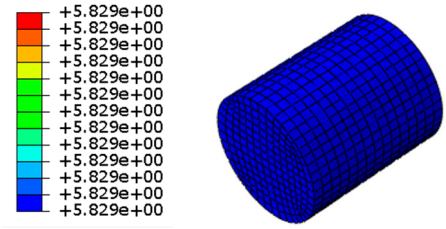

Figure 4. Fatigue life of steel wire used to confirm parameters (the values are the logarithm of the fatigue life base 10).

2.4. Comparison of Fatigue Life of a Single Steel Wire

2.4.1. Stress Distribution

Figure 5 shows the normal stress nephogram of the steel wire at the upper and lower limits of fatigue loading. At the lower limit of fatigue (the first stage), the normal stresses along the Z axis are all tensile stresses, with a maximum value of 647.2 MPa, indicating that the contact position between filling steel wires and the test steel wire produces a certain degree of stress concentration. The maximum normal stress along the Y axis is 1.2 MPa and the minimum is −100.2 MPa. The maximum normal stress along the X axis is 9.0 MPa and the minimum is −51.3 MPa. At the fatigue limit (the second stage), the normal stresses along the Z axis are all tensile stresses, and the maximum is 979.6 MPa. The maximum normal stress along the Y axis is 1.3 MPa and the minimum is −107.8 MPa. The maximum normal stress along the X axis is 9.163 MPa and the minimum is −51.3 MPa.

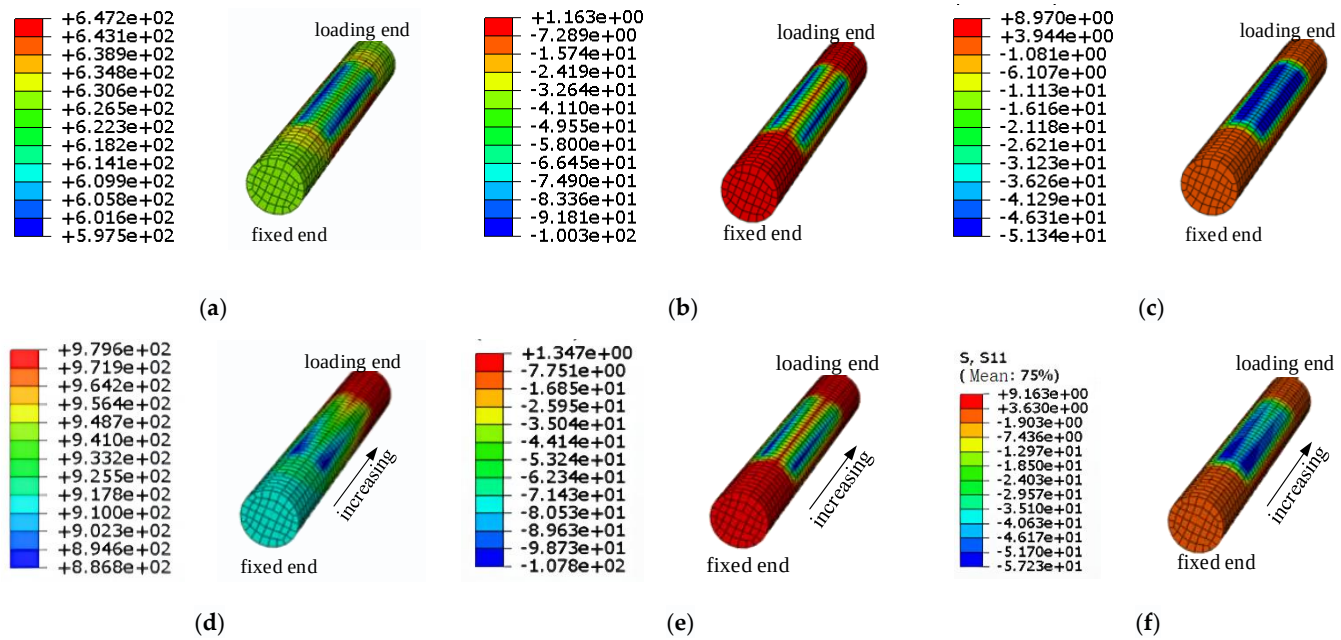

Figure 5. The normal stress distribution of local elements in the span of steel wire along all directions of the global coordinate system. Where, (**a**–**c**) are normal stress nephograms of steel wire along Z axis (axial direction), Y axis, and X axis, respectively, (**d**–**f**) are normal stress nephograms of steel wire along Z axis (axial direction), Y axis, and X axis, respectively, for fatigue upper limit time.

By comparing the normal stress nephograms of the two stages, it is not difficult to notice that the axial distribution of normal stress in all directions in the middle clamping region of the second stage increases from the fixed end to the loading end, while the axial distribution of normal stress in all directions in the middle clamping part of the first stage is uniform, which indicates that the filled wire and the center wire slip in the second stage, and the shear stress can no longer be ignored. Figure 6 shows the distribution of τ_{xz} and

τ_{yz}. It can be seen that the shear stress in the first stage is mainly concentrated at the end of the clamping region, while the range of the shear stress in the second stage gradually increases from the fixed end to the loading end, and the shear stress stops when it increases to about 6.4 MPa. This indicates that the relative slip degree between the center wire and the packed wire also increases gradually from the fixed end to the loading end.

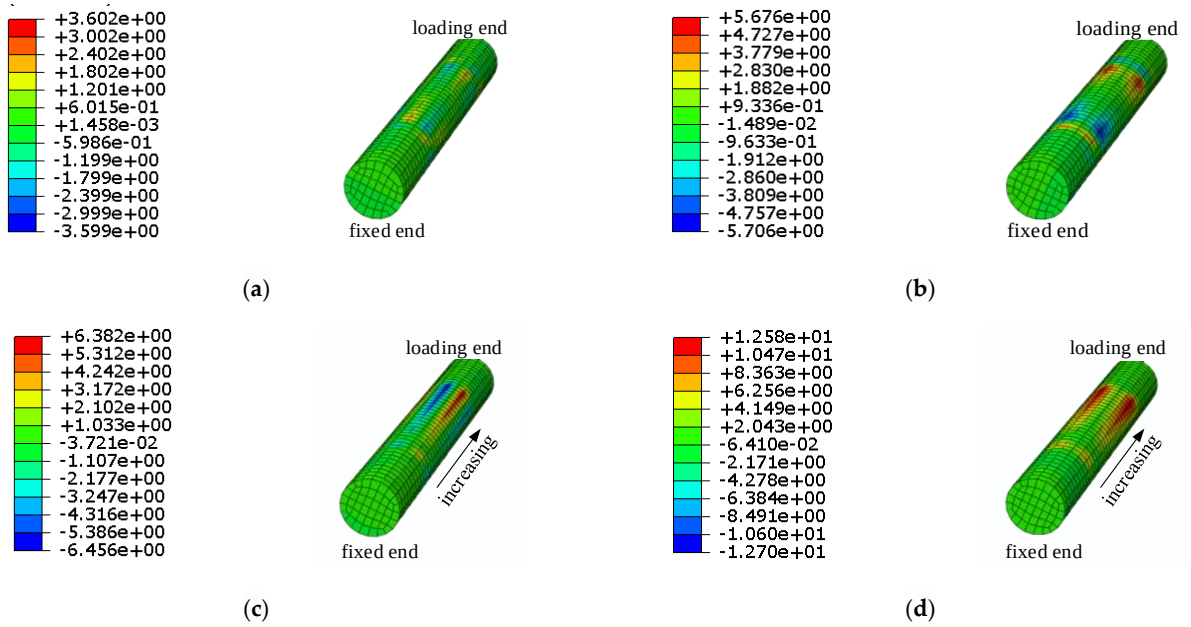

Figure 6. Cloud diagram of shear stress distribution. Here, (**a**) is τ_{xz} in the first stage, (**b**) is τ_{yz} in the first stage, (**c**) is τ_{xz} in the second stage, and (**d**) is τ_{yz}, in the first stage.

2.4.2. Fatigue Life

Figure 7 is the fatigue life of test steel wire obtained by simulating fatigue loading test of a single steel wire when the upper limit of uniform axial tensile stress load is 990.0 MPa and the stress range is 360.0 MPa. The holding area was the critical part, with a lifetime of $10^{5.527}$ (336,500) times, which was basically consistent with the test loading result of $10^{5.301}$ (200,000) times (the difference is 4.3% in logarithmic coordinate system). This indicated that it is reasonable to select 0.215 as friction coefficient and 1.15 as SN scale factor.

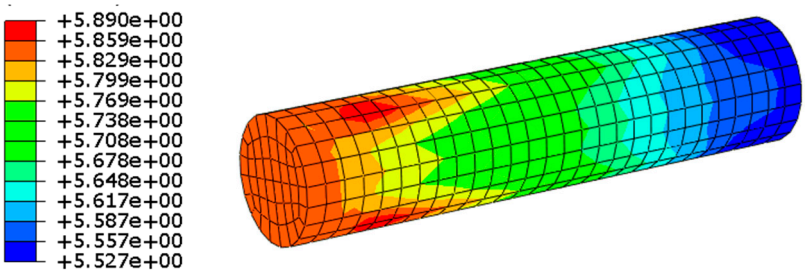

Figure 7. Fatigue life in the gripping area of a single wire (the values are the logarithm of the fatigue life base 10).

3. Fatigue Life Analysis of Main Cable Strand Wire at the Exit of Cable Saddle

3.1. Finite Element Modeling

The main cable specification of a suspension bridge is 5.65–127 × 247, and with five main cable ventilation pipes. The center curvature radius of the main cable at the saddle of the main pylon is R = 18 m; the width and height of a single strand channel are 62.5 mm and 64 mm, respectively. The width and height of a single strand channel are 62.5 mm and

64 mm, respectively. The facade of cable saddle and the cross-section of the cable saddle groove is shown in Figure 8a,b.

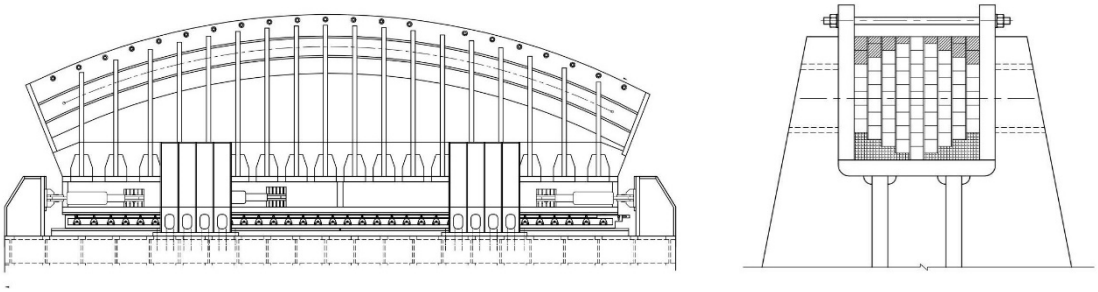

(**a**) (**b**)

Figure 8. Cable saddle structure form. (**a**) Facade. (**b**) Saddle groove profile.

In order to study the fatigue life of the main cable strand at the exit of the cable saddle, it is necessary to accurately solve the stress of the cable strand in the cable saddle. Secondary modeling is adopted in this study. In the first-level model, the main cable at the exit of the cable saddle is regarded as the multi-layer steel plate. The steel wire in the second-level model is in the form of actual section, and the interlaminar compressive stress of the first stage model is applied to the second stage model as load.

3.1.1. The First-Level Model

The first stage model takes the saddle groove in the middle of the cable saddle, located at the outlet of the cable saddle, with a central angle of 1°. The diameter of each wire in the first-level model is 5.65 mm. The saddle groove size was modeled according to the actual single-groove cable strand size of the main cable saddle. The width of the saddle was 62.15 mm, the depth was 60.23 mm, the width of the two sides of the baffle was 5 mm. As shown in Figure 9a, simplification was adopted, a single strand was divided into six layers, and the equivalent rectangular section size of each strand was the size of the outer contour of each strand.

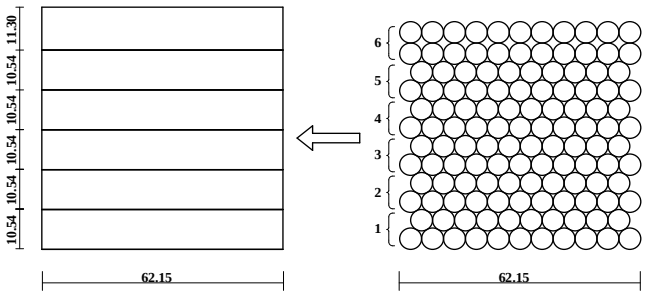

(**a**)

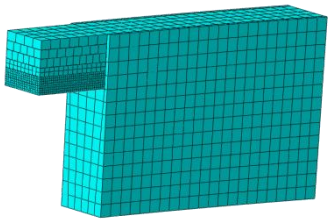

(**b**)

Figure 9. Model of main cable strand and saddle (the first-level model). (**a**) Equivalent section of strand wire. (**b**) Mesh generation.

Simplify Methods and Material Properties

When simplification was performed for each layer of cable strand, the following requirements were met: (1) Poisson's ratio before and after equivalent remains unchanged; (2) the ratio of the equivalent front and rear density is equal to the ratio of the actual wire to the equivalent rectangular section area, as is the conversion of the elastic modulus. The material properties are shown in Table 3.

Table 3. Model material property.

Material Property	Equivalent Steel Plate		Cable Saddle	Steel Wire
	First Five Layers	Sixth Layer		
Density (kg/m^3)	6.30×10^3	6.20×10^3	7.85×10^3	7.85×10^3
Elastic modulus (GPa)	168.7	164.9	210.0	210.0
Poisson ratio	0.3	0.3	0.3	0.3

Element Attributes and Meshing

Solid element C3D8R was used to simulate both steel plate and saddle groove. During mesh division, the stress of the first layer of cable strands at the bottom of the saddle outlet was analyzed emphatically. Considering the convergence of the element, more detailed mesh division was carried out for the bottom two layers of cable strands, and the size of the wire element was 0.3 mm. Figure 9a is a schematic diagram of grid division.

Contact Properties and Boundary Conditions

After calculation, the interactions between each layer of steel wire and between steel wire and saddle groove were set as surface-to-surface contact, and the boundary conditions at the bottom and side of the saddle groove were set as consolidation (U1 = U2 = U3 = UR1 = UR2 = UR3 = 0). The solid unit of the main cable wire is coupled by a rigid surface set at the end of the cable saddle. The tensile fatigue load of the cable strand is applied at the loading end in the form of pressure, the upper limit of fatigue is 900.0 MPa, and the stress range is 156 MPa. The effect of the upper strand was simulated by applying a pressure of 40.9 MPa at the top of the strand.

Finally, the contact compressive stress between the first and second layers of steel plates is calculated to be 44.7 MPa, which is loaded on the second-stage model as a load.

3.1.2. The Second-Level Model

In the second-level model, solid units are used to simulate the cable saddle and the steel wire in the saddle groove, and the single steel wire at the bottom of the saddle groove is simulated in the form of actual cross-section, as shown in Figure 10. Among them, five steel wires are arranged in two layers, with a diameter of 5.65 mm and a length of 80 mm. The cable saddle is simulated as a "U" shaped saddle groove, with a thickness of 5 mm, a length of 40 mm, and a width of 16.95 mm in the groove, which can accommodate three steel wires arranged in parallel. The upper steel wire was simulated as a steel plate, 5 mm thick, 16.95 mm wide, and 40 mm long.

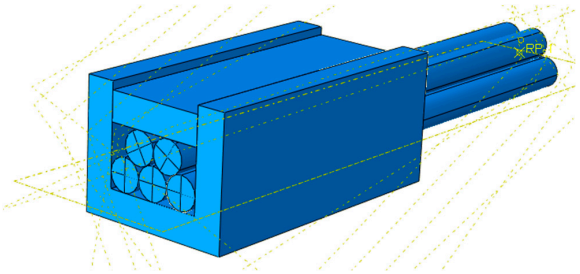

Figure 10. Partial model of saddle and wire (the second-level model).

Material Property

As is shown in Table 3, the material properties of the steel wire and saddle groove adopt the actual material properties; the contact attributes were set as in Table 3.

Element Attributes and Meshing

Solid element C3D8R was used to simulate both steel plate and saddle groove. During mesh division, the mesh size of each component of the model was 0.1 mm, considering the requirement of unit convergence

Contact Properties and Boundary Conditions

In the second-level model, the contact properties between cable strands are set in the same way as that of the first stage model. The boundary conditions at the bottom and side of the saddle groove were set as consolidation. The fatigue tensile load on cable strands is applied at the loading end in the form of pressure, with the upper fatigue limit of 900.0 MPa and the stress range of 156.0 MPa. The action of the upper steel wire is simulated as the compressive stress loaded on the upper steel plate, and the size is 44.7 MPa.

3.2. Fatigue Life Prediction of Main Cable at Cable Saddle Outlet

3.2.1. Stress Distribution of Steel Wire

Figure 11 shows the normal stress nephograms of the upper and lower limits of the steel wire under fatigue loading. At the lower limit of fatigue (the first stage), the axial uniform tensile load is 744.0 MPa. The maximum normal stress along the Z axis (axial direction) is tensile stress, and the maximum normal stress along the Y axis is 218.3 MPa and the minimum normal stress is −488.2 MPa. The maximum and minimum normal stresses along the X axis are 154.7 MPa and −180.0 MPa. At the fatigue limit (the second stage), the axial uniform tensile load is 900.0, in which the normal stress along the Z axis is tensile stress, and the maximum is 1171.0 MPa. The maximum normal stress along the Y axis is 266.5 MPa and the minimum is −593.7 MPa. The maximum and minimum normal stresses along the X axis are 188.3 MPa and −219.4 MPa, respectively.

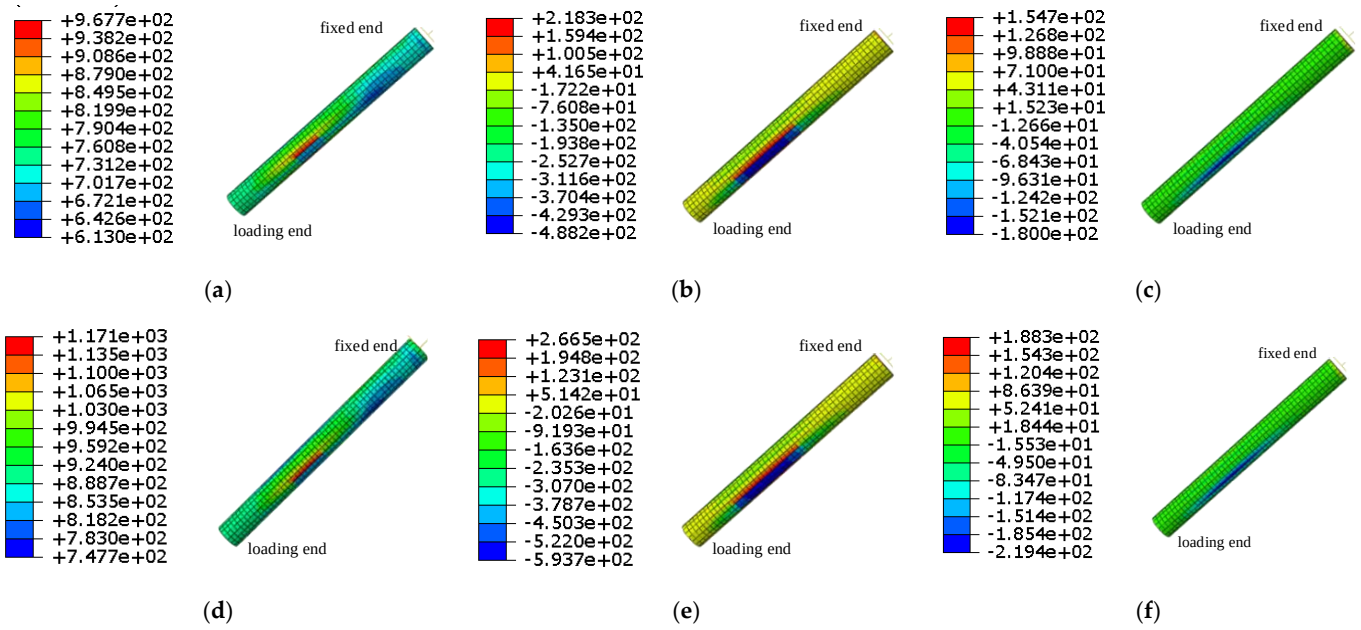

Figure 11. The normal stress of the wire along all directions of the integral coordinate system, where (**a**–**c**) are normal stress nephograms of steel wire along Z axis (axial direction), Y axis, and X axis, respectively, and (**d**–**f**) are normal stress nephograms of steel wire along Z axis (axial direction), Y axis and X axis, respectively, for fatigue upper limit time.

3.2.2. Fatigue Life

The input parameters in the fatigue analysis process are consistent with the simulation of single steel wire fatigue test. As shown in Figure 12, the fatigue life of the bottom center steel wire of the main cable when the upper limit of uniform axial tensile stress is 900.0 MPa and the stress amplitude is 156.0 MPa. The critical part occurred in the contact between the steel wire and the bottom of the saddle groove, which was consistent with the engineering practice and had a life of 4.78 million times, indicating that the 2200 MPa steel wire had good durability and could work at the outlet of the cable saddle for a long time to meet the needs of the actual project.

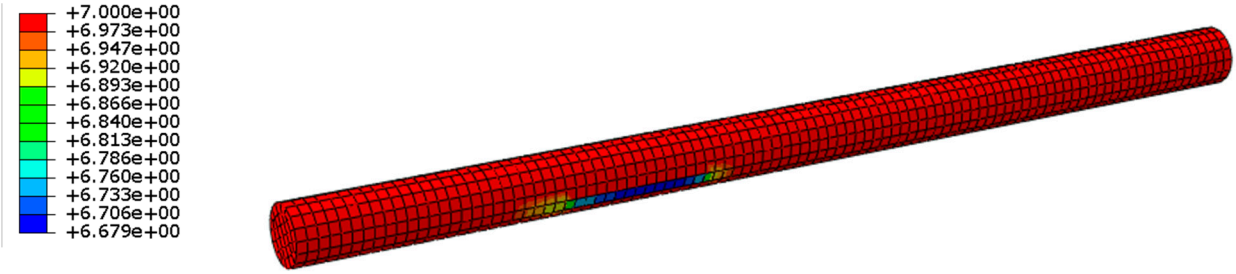

Figure 12. Fatigue life of 2200 MPa high-strength steel wire.

4. Conclusions

In this paper, the values of friction coefficient and SN scale factor in finite element simulation and fatigue life analysis were determined by fatigue loading test of a single steel wire, and then the stress state of 2200 MPa main cable steel wire at the saddle outlet was simulated; the fatigue life analysis was carried out, and the following conclusions were obtained:

(1) In the fatigue loading test, the filling and holding steel plate for clamping amplify the stress concentration of the steel wire, which is inconsistent with the stress state of the steel wire at the outlet position of the cable saddle in the actual engineering.
(2) It is reasonable to adopt 0.21 as friction coefficient in finite element simulation and 1.15 as SN scale factor in fatigue life analysis, which can effectively simulate the stress state of the main cable steel wire.
(3) Through fatigue life analysis based on ABAQUS/FE-SAFE, it is determined that the critical position of the main cable wire at the outlet of the cable saddle is the contact between the bottom wire and the outlet of the cable saddle, and the fatigue life is 4.78 million times. The 2200 MPa grade steel wire has good durability and can work at the outlet of the cable saddle safety to meet the needs of the actual project.

Author Contributions: Methodology, Z.Z.; Validation, J.Z.; Formal analysis, S.L.; Resources, H.L.; Data curation, L.W.; Writing – review & editing, H.S. All authors have read and agreed to the published version of the manuscript.

Funding: This research was funded by Jiangsu Provincial Transportation Engineering Construction Bureau (ZG-KT-3-7-1).

Institutional Review Board Statement: Not applicable.

Informed Consent Statement: Not applicable.

Data Availability Statement: Not applicable.

Acknowledgments: The authors would like to gratefully acknowledge the financial support by the Jiangsu Provincial Transportation Engineering Construction Bureau (ZG-KT-3-7-1).

Conflicts of Interest: The authors declare no conflict of interest.

References

1. Makii, K.; Yaguchi, H.; Kaiso, M.; Ibaraki, N.; Miyamoto, Y.; Oki, Y. Influence of Si on nano sub-structure of cementite lamellae in pearlitic steel wires. *Scr. Mater.* **1997**, *37*, 1753–1759. [CrossRef]
2. Benidir, A.; Flamand, O.; Gaillet, L.; Dimitriadis, G. Impact of roughness and circularity-defect on bridge cables stability. *J. Wind Eng. Ind. Aerodyn.* **2015**, *137*, 1–13. [CrossRef]
3. Krkoška, L.; Moravčík, M.; Zgútová, K.; Neslušan, M.; Uhričík, M.; Bahleda, F.; Pitoňák, M. Investigation of barkhausen noise emission in steel wires subjected to different surface treatments. *Coatings* **2020**, *10*, 912. [CrossRef]
4. Mohareb, S.; Goldack, A.; Schlaich, M.; Walbridge, S. Effect of Relative Displacement of Strands Bent Over Circular Saddles on Fatigue Life Under Fretting Conditions. In *High Tech Concrete: Where Technology and Engineering Meet*; Hordijk, D.A., Luković, M., Eds.; Springer International Publishing: Cham, Switzerland, 2018; pp. 2307–2315. ISBN 978-3-319-59470-5.
5. Wu, Y.; Ya, G.; Dai, X.; Zhang, X. Key techniques of 1960MPa steel wire and wire strand for main cable of Second Humen Bridge. *Bridge Constr.* **2018**, *48*, 5–10.
6. Song, H.; Wang, X. Zhoushan Xihoumen Bridge with the World Record Span Length of Steel Box Girder, China. *Struct. Eng. Int.* **2010**, *20*, 312–316. [CrossRef]
7. Lu, J.; Cai, Y.; Xue, H.; Zhang, Y. Research of static load performance test of 1960 MPa super strengthzinc aluminum alloy coated steel wire main cable strand. *Met. Prod.* **2017**, *43*, 37–43.
8. Chen, H.; Song, S.; Zhang, H.; Hang, D. Key manufacturing technology of 2 060 MPa Zn-Al-Mg alloy coated steel wire strands utilized in Lingdingyang Bridge. *Bridge Constr.* **2022**, *52*, 21–27.
9. Wang, L.; Shen, R.; Bai, H.; Wang, Y. Test for slip behavior and mechanical characteristics between main cable and saddle in suspension bridges. *China J. Highw. Transp.* **2018**, *31*, 75–83+103.
10. Su, Y.; Fu, Y.; Xie, J.; Chen, L.; Huang, A. cable-saddle anti-slipping test of AS method suspension bridges. *J. Chongqing Jiaotong Univ.* **2022**, *41*, 66–73. [CrossRef]
11. Li, H.; Zheng, G.; Chen, C. Determination of friction coefficients between steel wires in stay cables. *J. Chongqing Jiaotong Univ.* **2011**, *30*, 196–199.
12. Dai, X.; Wang, L.; Wang, C.; Wang, X.; Shen, R. Anti-slip scheme of full-vertical friction plate for multi-pylon suspension bridge. *J. Zhejiang Univ.* **2019**, *53*, 1697–1703. [CrossRef]
13. Guo, Z.; Hua, X.; Xue, H. Experimental study on fatigue performance of 2100MPa high strength main cable strands. *Highway* **2020**, *65*, 216–219.
14. Lee, B. Fatigue analysis under variable amplitude loading using an energy parameter. *Int. J. Fatigue* **2003**, *25*, 621–631. [CrossRef]
15. Garud, Y.S. A new approach to the evaluation of fatigue under multiaxial loadings. *J. Eng. Mater. Technol.* **1981**, *103*, 118–125. [CrossRef]
16. Varvani-Farahani, A. A new energy-critical plane parameter for fatigue life assessment of various metallic materials subjected to in-phase and out-of-phase multiaxial fatigue loading conditions. *Int. J. Fatigue* **2000**, *22*, 295–305. [CrossRef]
17. Kim, K.S.; Park, J.C.; Lee, J.W. Multiaxial fatigue under variable amplitude loads. *J. Eng. Mater. Technol.* **1999**, *121*, 286–293. [CrossRef]
18. He, G.; Chen, C.; Gao, Q.; Sun, X.; Shen, Z. Study on mul-tiaxial low cycle fatigue under nonproportional loading of 316L stainless steel. *Chin. J. Mech. Eng.* **1999**, *35*, 47. [CrossRef]
19. Zhang, G.; Gengqiang, P.U.; Wang, C. Fatigue life prediction of crankshaft made of material 48MnV based on fatigue test, dynamic simulayion and FEA. *Chin. J. Mech. Eng.* **2006**, *19*, 307–311. [CrossRef]
20. Brown, M.W.; Miller, K.J. A Theory for Fatigue Failure under Multiaxial Stress-Strain Conditions. *Proc. Inst. Mech. Eng.* **1973**, *187*, 745–755. [CrossRef]
21. Brown, M.W.; Miller, K.J. High temperature low cycle biaxial fatigue of two steels. *Fatigue Fract. Eng. Mater. Struct.* **1979**, *1*, 217–229. [CrossRef]
22. Fatemi, A.; Socie, D.F. A critical plane approach to multiaxial fatigue damage including out-of-phase loading. *Fatigue Fract. Eng. Mater. Struct.* **1988**, *11*, 149–165. [CrossRef]
23. Zhao, Y.; Song, Y. Multi-axial fatigue life prediction model in elliptic equation form. *Chin. J. Mech. Eng.* **2009**, *45*, 312–316. [CrossRef]
24. Wu, Z.; Hu, X.; Song, Y. Multi-axial fatigue life prediction model based on maximum shear strain amplitude and modified SWT parameter. *Chin. J. Mech. Eng.* **2013**, *49*, 59–66. [CrossRef]
25. Jia, R.; Wang, C. Analysis on fretting fatigue characteristics of steel strand cable based on SWT method. *Chin. Q. Mech.* **2020**, *41*, 657–665. [CrossRef]
26. Ma, L. Study on fatigue properties of domestic1860 low relaxation prestressed steel strand. *Railw. Stand. Des.* **2000**, *5*, 21–23. [CrossRef]
27. Li, Q.; Ye, Z.; Huang, R.; Liu, Z.; Liu, X. Research on multi-axial fatigue analysis method of transmission line tension string fittings based on Abaqus/Fe-Safe. *Chin. Q. Mech.* **2022**, *43*, 659–669. [CrossRef]
28. He, Y.; Zhou, R.; Hu, L.; Cao, Z.; Xiang, Y. Fatigue properties of bolt connectors in HERC. *J. Chang. Univ.* **2021**, *41*, 95–105. [CrossRef]